JOURNAL OF MATERIALS SCIENCE 35 (2000) 2015–2027

Synthesis and characterization of $Cu_2O{\cdot}TeO_2$ and $CuI{\cdot}Cu_2O{\cdot}TeO_2$ glasses

B. V. R. CHOWDARI, K. L. TAN, FANG LING
Department of Physics, National University of Singapore, Singapore 119260
E-mail: phychowd@nus.edu.sg

$Cu_2O{\cdot}TeO_2$ and $CuI{\cdot}Cu_2O{\cdot}TeO_2$ glasses were synthesized and characterized by complex impedance measurement, Raman spectroscopy, X-ray photoelectron spectroscopy, and atomic force microscopy techniques. Samples of the binary and the ternary systems are found to have both Cu^+ and Cu^{2+} with their relative concentration being composition dependent. Bonds like -O-Cu^{2+}-O-, leading to the formation of bridging oxygen are found to form in the binary system. Structural units like $(Te_3O_8^{4-})_n$ are also found to form when Cu_2O content is high in the binary system. Phase separation is observed in the ternary system. The glass structure and hence the ionic conduction behavior are found to depend upon chemical composition. When CuI content exceeds 60 mol %, the crystalline phase of α-CuI gets stabilized at room temperature, thus causing the enhancement in conductivity.

1. Introduction

Ionic conducting glasses have been the subject of investigation for a long time and a large number of researchers have put in lots of efforts in exploring new glass systems [1, 2]. These materials have advantages over their crystalline counterparts, because of the possibility of forming glasses in large composition range with isotropic properties. Among the glassy electrolytes developed so far, silver ion ones are ranked as primary because of their high ionic conductivity and easy synthesis process. However, the high cost of silver based glasses and low voltage achievable in solid state battery applications have led researchers to pursue studies on other ionic conducting glass systems. Similarity of electron configuration (d^{10}) between Ag^+ and Cu^+ and also the relatively small ionic radius of Cu^+ (0.96×10^{-10} m) as compared to that of Ag^+ (1.26×10^{-10} m) [3] make cuprous ion based glasses interesting. Because of the difficulties concerning cuprous glass synthesis, only a limited number of cuprous glass systems have been reported and they usually consist of cuprous halide, cuprous oxide and phosphorus-, molybdenum- or tungsten-oxide as glass former. Unlike other monovalent ion based glasses, it is difficult to form copper ionic conducting glasses with normal glass formers such as B_2O_3, P_2O_5, V_2O_5 etc. [4, 5]. Therefore, in order to extend our knowledge on synthesis and characterization of copper based glass systems through the study of their structure and properties, we have attempted to study different copper based glass systems. We have found that the cuprous iodide and cuprous oxide as starting materials can indeed form glasses with tellurium oxide as a glass former.

Tellurium oxide is a conditional glass former and hence only a limited number of studies are made on the tellurite based system. Its attractive properties arise from its special structural characteristics [6]. It has been demonstrated that amorphous TeO_2 and crystalline α-TeO_2 consist of a three dimensional network of TeO_4 structural units. The TeO_4 unit is a trigonal bipyramid (tbp) in which one of the Te sp^3d hybrid orbitals is occupied by an electron lone pair while the other two equatorial positions (O_{eq}) and two axial positions (O_{ax}) are occupied by four oxygen atoms. Introduction of the modifier into TeO_4 network would break Te-O-Te bonds and at the same time would give rise to new structural units such as TeO_3 with nonbridgining oxygen. The TeO_3 unit is a trigonal pyramid (tp), in which an electron lone pair occupies one of the Te sp^3 hybrid orbitals. Many researchers [4–12] have studied Tellurite glasses with different modifiers such as Li_2O, Ag_2O, K_2O, etc. But, to our knowledge, tellurite glass containing copper ions has not been studied so far. Hence, we have attempted to synthesize and characterize copper based tellurite glasses and also study their interesting electrical, thermal and surface characteristics [7–12].

In this paper, we report the preparation of the $Cu_2O{\cdot}TeO_2$ and $CuI{\cdot}Cu_2O{\cdot}TeO_2$ glass systems and also the results obtained from the studies by X-ray photoelectron spectroscopy (XPS), Raman spectroscopy, atomic force microscopy(AFM) and complex impedance techniques. It is concluded that the resulting samples contained both Cu^+ and Cu^{2+} and a phase separation occurred in $CuI{\cdot}Cu_2O{\cdot}TeO_2$ system when the CuI content was relatively high. We have also found that the crystalline phase of α-CuI got stabilized at room

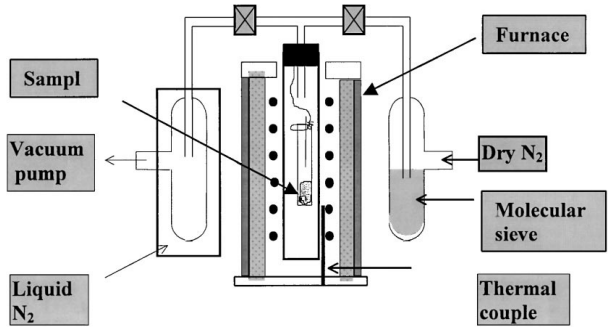

Figure 1 The schematic diagram of experimental set up for glass sample preparation. (1) Quartz crucible; (2) Quartz tube as vacuum chamber.

temperature by glass matrix and hence became responsible for high ionic conductivity.

2. Experimental techniques

Reagent grade CuI, Cu_2O and TeO_2 (Fluka chemika) were used as starting materials. A mixture of these chemicals of appropriate composition was melted in a quartz tube at 750°C for 15 minutes in a vacuum facility (10^{-3} torr) as illustrated in Fig. 1 [13]. In general, the quartz tube which contains molten material was quickly taken out of the vacuum and the melt was quenched in air using a twin-roller set-up, as it provides higher quenching speed and larger glass forming region [9]. However, as described later, melting and quenching in vacuum did not give any significantly different results.

X-ray diffraction (XRD), using a Philips PW1710 diffractometer, was used to check the amorphous nature of the glass specimens. The Cu-K_α X-ray source ($\lambda = 1.541$ Å) was used. The glass transition temperature (T_g) was measured by differential scanning calorimeter (DSC, Shimadzu DSC-50) with the glass specimens scanned at a heating rate of 10 °C/min.

A Ranishew Raman imaging microscopy had been used for Raman spectroscopy measurements and the experimental detail was given elsewhere [14]. Raman spectra were recorded in the 200 to 1200 cm^{-1} ranges. The specimens in the form of powder were excited by 488-nm light from an argon-ion laser operated at about 200-mW power. The curve fitting method was used to fit the Raman spectra into symmetric Gaussian peaks. The program with Ranishew Raman microscope system applies the least square method to optimize the position and intensities of the Gaussian peaks, while keeping the full width half maximum (FWHM) of the peaks constant as 40 cm^{-1}.

Selected glass specimens were analyzed by X-ray photoelectron spectroscopy (XPS)(VG scientific ESCALAB MKII) with a Mg-K_α X-ray source ($h\nu$ = 1253.6 eV). For the XPS measurements, glass powder was used and the samples were powdered just before the experiments to avoid surface oxidation. The electron energy analyzer of the spectrometer was set at constant pass energy of 20 eV. All the peaks were referenced to the C 1s peak of binding energy 284.6 eV, which appears as a surface contamination.

Electrical conductivity measurements were performed using the complex impedance method in the frequency range 10 to 10^6 Hz. The instrument was composed of a frequency response analyzer (Solartron 1255) and an electrochemical interface (Solartron 1286). Those glasses that contained cuprous halide were found to have higher conductivity and hence the electrical conductivity measurements were made in the temperature range −70 to +25 °C. The conductivity of the binary glass system was measured from the room temperature to about 50 °C less than T_g. For electronic conductivity measurements, glass pellets on which one side was coated with gold as a blocking electrode and the other side with copper as a non-blocking electrode were used. Wagner's polarization method was used to measure the electronic conductivity making use of an electrometer (Keithley 617) [15].

Atomic force microscopy (AFM, Dimension TM3000, Digital Instruments Inc.) and scanning electron microscopy (SEM, JEOL JSM-35CF) measurements on selected samples were carried out to confirm the microstructure of the glass samples. AFM [16] utilizes a sharp tip fixed on a cantilever to scan the sample surface and the force between the tip and the sample surface causes the cantilever to bend. This displacement is detected by a laser sensor, revealing the topography of the sample surface. In this experiment, the tapping mode was used because this mode could give as high a resolution as contact mode. All the samples were etched by diluted HCl solution to reveal the sub-micron structure of the glass samples.

3. Experimental results

3.1. Glass forming region, DSC and AFM studies

The glass forming region of $x\mathrm{Cu_2O}\cdot(1-x)\mathrm{TeO_2}$ and $x\mathrm{CuI}\cdot(1-x)[y\mathrm{Cu_2O}\cdot(1-y)]\mathrm{TeO_2}$ systems is shown in Fig. 2. XRD study confirms that for the binary system the specimens with $x = 10$ to 40 mol% are in glassy state and the specimen with $x = 50$ mol% shows only a small fraction of crystalline state. This crystalline phase is identified as Cu_2O. The glass transition temperatures (T_g) for various compositions are listed in Table I. It is found that T_g increases with increase in Cu_2O content.

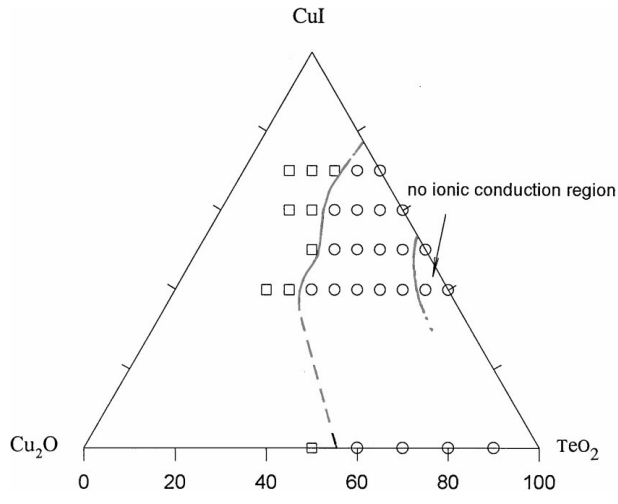

Figure 2 The glass forming region of $x\mathrm{Cu_2O}\cdot(1-x)\mathrm{TeO_2}$ and $x\mathrm{CuI}\cdot(1-y)\mathrm{Cu_2O}\cdot(1-x-y)\mathrm{TeO_2}$ systems. □ Partial crystallized ○ Glass.

TABLE IA Electrical properties and glass transition temperatures (T_g) of xCu$_2$O·$(1-x)$TeO$_2$ glasses

X	T_g	σ_e (S cm^{-1})	σ_{298_K} (S cm^{-1})	Log σ_0	E_{act} (eV)
0.1	301.1	4.05×10^{-14}	∼	∼	∼
0.2	308.2	4.57×10^{-12}	∼	∼	∼
0.3	315.2	3.24×10^{-11}	∼	∼	∼
0.4	329.2	2.05×10^{-9}	$(1.18 \pm 0.06) \times 10^{-7}$	1.38 ± 0.14	0.33 ± 0.01
0.5	331.6	2.24×10^{-9}	$(5.34 \pm 0.01) \times 10^{-7}$	0.94 ± 0.19	0.32 ± 0.01

TABLE IB Electrical properties of xCuI·yCu$_2$O·$(1-x-y)$TeO$_2$ glasses

x	y	$\sigma_{electron}$ (S cm^{-1})	$(\sigma_{298K} \pm 0.17) \times$ (10^{-4} S cm^{-1})	Log $\sigma_0 \pm$ 0.15	$E_{act} \pm$ 0.01 (eV)
0.40	0.00	4.28×10^{-12}	∼	∼	∼
0.40	0.05	2.89×10^{-11}	∼	∼	∼
0.40	0.10	3.02×10^{-9}	∼	∼	∼
0.40	0.15	2.54×10^{-8}	2.31	1.02	0.28
0.40	0.20	3.02×10^{-7}	2.55	1.48	0.30
0.40	0.25	3.15×10^{-7}	0.48	4.05	0.50
0.40	0.30	6.51×10^{-7}	1.40	4.38	0.49
0.40	0.35	9.42×10^{-7}	1.62	4.12	0.47
0.40	0.40	9.22×10^{-7}	0.11	3.71	0.51
0.70	0.00	2.03×10^{-7}	0.78	4.49	0.51
0.70	0.05	2.27×10^{-6}	2.99	4.61	0.48
0.70	0.10	1.62×10^{-6}	10.20	5.69	0.51
0.70	0.15	1.10×10^{-6}	4.23	1.40	0.28
0.70	0.20	8.69×10^{-5}	42.10	0.65	0.18

The ternary system has relatively large glass forming region similar to that of LiCl·Li$_2$O·TeO$_2$ [17]. The AgI·Ag$_2$O·TeO$_2$ glass system [18] has a narrow glass forming region as compared to those of its Cu and Li counterparts. The cuprous iodide tends to crystallize when Cu$_2$O content exceeds certain level especially when CuI concentration is high. From the peak position and intensity ratio of XRD peaks, it is confirmed that the crystalline phase is α-CuI. SEM study shows that the crystallites are formed in the glass matrix and their average diameter is about 104.8 nm (Fig. 3).

We have found that it is, in general, quite difficult to determine T_g in the ternary system. This observation is quite similar to that we had made earlier in the studies of CuI·AgI·Cu$_2$MoO$_4$·CuPO$_3$ system [13]. We believe that the phase separation that occurs in these systems lead to the interference between glass transition and crystallization processes and hence made it more difficult to observe the transition temperature.

Fig. 4 shows the microstructure of some typical glass samples of the ternary system obtained by AFM. The structural characteristics of these materials could be visualized as if they were composed of many droplets and these droplets form very dense clusters of different sizes.

3.2. Raman spectra

The Raman spectra of xCu$_2$O·$(1-x)$TeO$_2$ (x: 0.1 ∼ 0.5) glasses are shown in Fig. 5. The spectra had a band at about 440 cm^{-1} and a broad doublet band in the 600 to 800 cm^{-1} regions. The doublet band could be resolved into four bands with maximum lying at about 620, 660, 720 and 780 cm^{-1} (D to A). Relative intensity of these bands was found to change with the change in Cu$_2$O content. In order to see the structure change tendency, we defining the fractional area of a particular peak as the ratio of the area under that peak and the total area under all peaks. We found that the fractional area of bands at 440 and 660 cm^{-1} decreased and that of bands at 620, 720 and 780 cm^{-1} increased with increasing x from 10 to 30 mol %. These changes

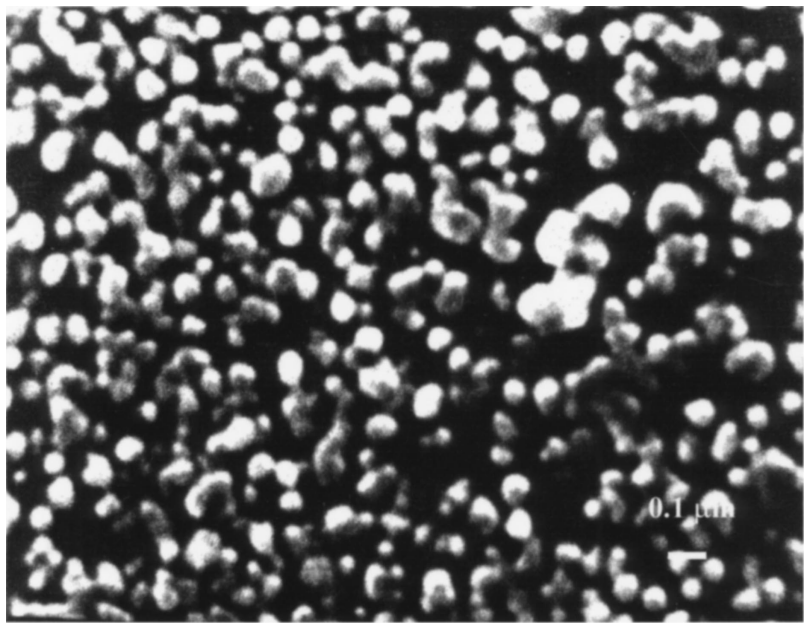

Figure 3 SEM images of α-CuI crystallites in glass of 0.7CuI·0.1Cu$_2$O·0.2TeO$_2$.

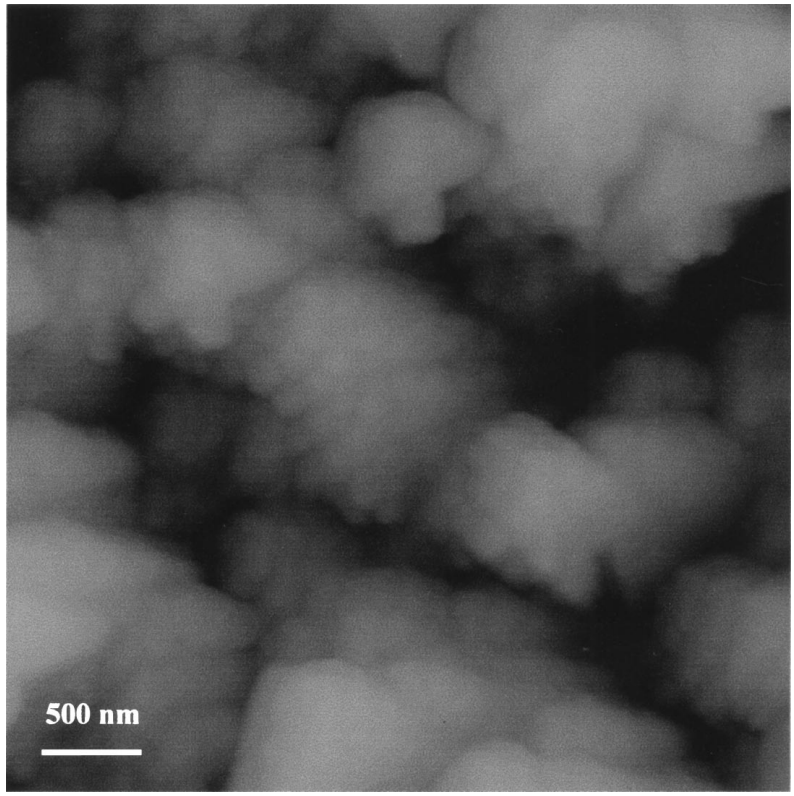

(a)

(b)

Figure 4 AFM observations of the glasses of (a), (b) $0.4CuI{\cdot}0.6TeO_2$; (c) $0.4CuI{\cdot}0.2Cu_2O{\cdot}4TeO_2$. (*Continued)*

are quite similar to the published data on other binary systems of similar composition range [19, 20]. However, when x increases from 30 to 50 mol %, a new band is observed at 400 cm^{-1} (F in Fig. 5) which strongly suggests that a new vibration mode appears and the intensity of this band increases with the increase in x within 30 to 50 mol% range. The fractional area of the bands at 440, 660, 720 and 780 cm^{-1} decreases whereas that at 620 cm^{-1} increases with increase in x from 30 to 50 mol%.

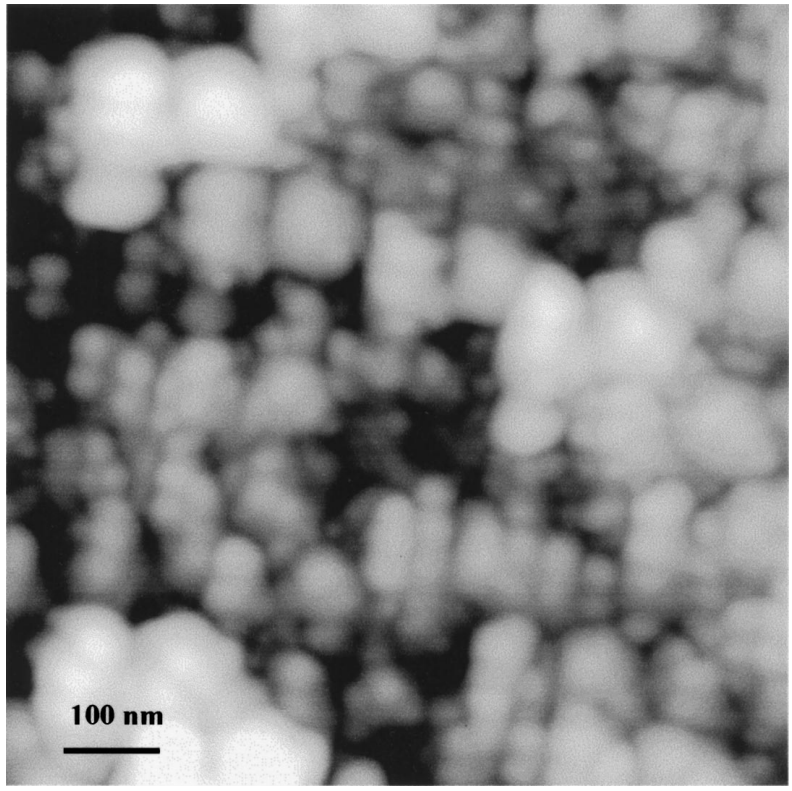

(c)

Figure 4 (Continued.)

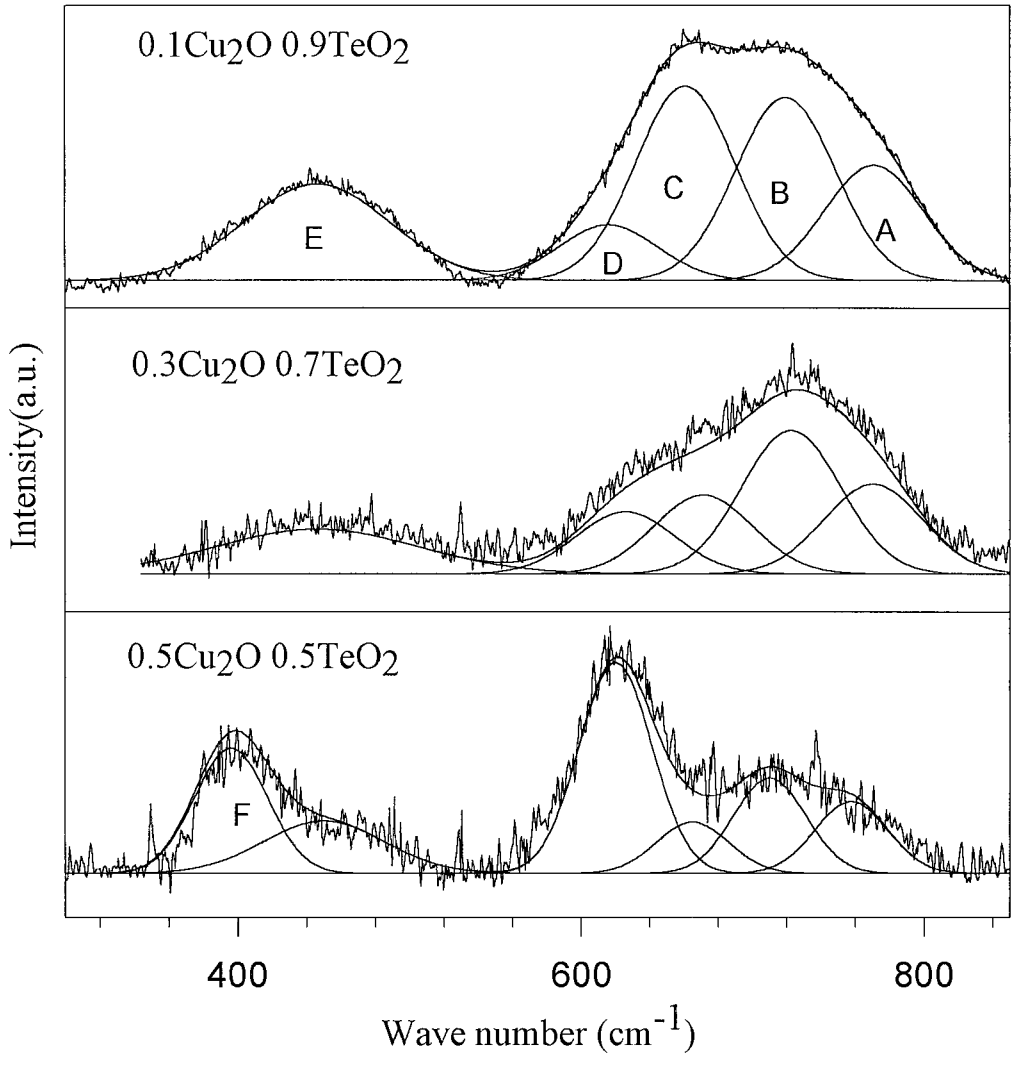

Figure 5 The Raman spectra and the deconvoluted peaks of $Cu_2O{\cdot}TeO_2$ glass system.

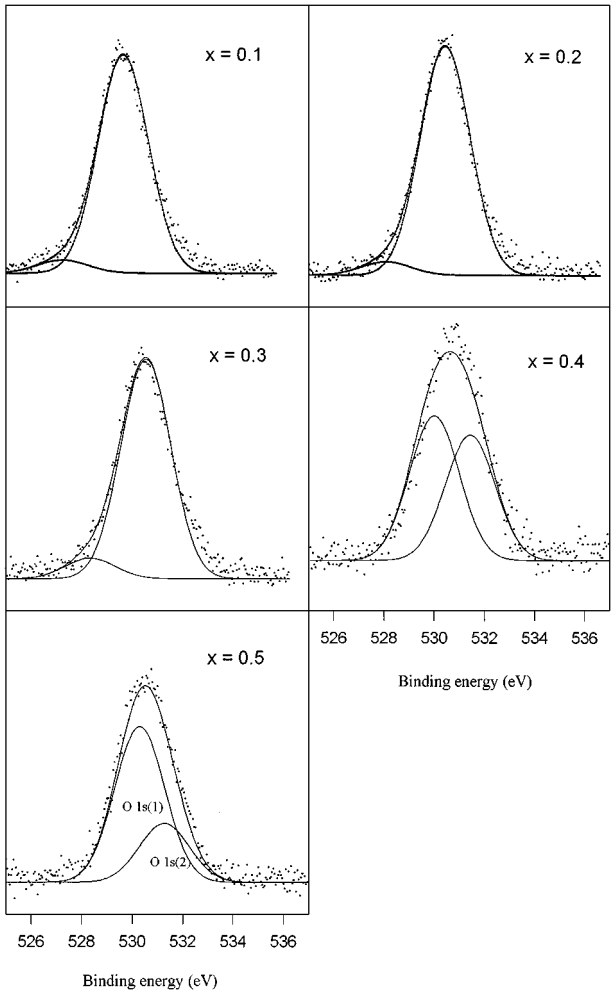

Figure 6 The O 1s core-level spectra of the $x\mathrm{Cu_2O}\cdot(1-x)\mathrm{TeO_2}$ glass system.

The ternary $\mathrm{CuI}\cdot\mathrm{Cu_2O}\cdot\mathrm{TeO_2}$ glasses have almost the same Raman spectral characeristics as the binary system. However, no 400 $\mathrm{cm^{-1}}$ band is observed and the 620 $\mathrm{cm^{-1}}$ band does not change as in the binary system. The Raman bands due to cuprous halide are within the far infrared range and hence can not be reported here.

3.3. X-ray photoelectron spectroscopy studies

Figs 6 and 7 show the O 1s, Cu 2p and Te 3d XPS spectra of the $\mathrm{Cu_2O}$-$\mathrm{TeO_2}$ system and the corresponding binding energies are listed in Table II. The O 1s spectra of the binary system can be fitted into two Gaussian peaks referred to as O 1s(1) and O 1s(2) in the order of increasing binding energy. The binding energies of O 1s(1) and O 1s(2) are about 528 and 530 eV respectively, for glasses with x less than 0.3. As x increased to 0.4 or 0.5, the binding energies of these two core-level electrons shifted to 530 and 531 eV, respectively. The peak-area ratio of O 1s(1) to total O 1s, referred to as $F(A)$, is a useful parameter and the values are tabulated in Table II. It was very clear that as for $x \leq 0.3$, the parameter $F(A)$ was only around 0.086 and as x is greater than 0.4 the $F(A)$ jumps to 0.349 and higher. The Te 3d peak could be fitted into two Gaussian peaks: one minor peak at about 573 eV and one dominant peak at about 575.4 eV (Fig. 7c). This minor peak shows very little changes with composition. In this study, we did not found that the Te 3d shows several peaks corresponding to different structural units, as reported for some binary tellurite glass systems [21].

The spectrum of the observed Cu 2p core-level electrons consists of two peaks with the binding energies at about 934 and 954 eV. Each of these two peaks has been fitted into two component peaks labeled as A and B, as shown in Fig. 7. The average separation between A and B is 1.6 and 2.6 eV for doublets fitted from the 934 and 954 eV peaks, respectively. In addition to the peaks at about 934 and 954 eV, the spectrum consists of a peak at about 942 eV. The intensity of this peak is found to change with the intensity of 934 eV peak. For the curve fitting of O 1s, Te 3d, Cu $2p_{1/2}$ and Cu $2p_{3/2}$ into Gaussian peaks, we use the same full width half maximum (FWHM) of 1.4, 1.3 and 1.9 eV, respectively, for all peaks appropriate to the particular element O, Te and Cu. XPS spectra of various core-level electrons including that of I 3d in $\mathrm{CuI}\cdot\mathrm{Cu_2O}\cdot\mathrm{TeO_2}$ system have also been recorded and the resulting data on binding energies are listed in Table III.

3.4. Electrical and electronic conductivity measurement

Fig. 8 shows plots of log σ vs. $1000/T$ for $x\mathrm{Cu_2O}\cdot(1-x)\mathrm{TeO_2}$ with $x = 0.4$ and 0.5, and $0.4\mathrm{CuI}\cdot y\mathrm{Cu_2O}\cdot(0.6-y)\mathrm{TeO_2}$ and $0.7\mathrm{CuI}\cdot y\mathrm{Cu_2O}\cdot(0.3-y)\mathrm{TeO_2}$ systems with $y = 0.15$ to 0.4 and 0 to 0.2, in increments of 0.05 respectively. The activation energy, pre-exponential factor, and the conductivity ($\sigma_{298\mathrm{K}}$) were calculated and tabulated in Tables IA and B. The measured data on the electronic conductivity were also listed in Tables IA and B. It may be noted that when $\mathrm{Cu_2O}$ content was less than 30 mol%, the electrical conductivity of glass specimens was so low that our present measuring instrument was not able to detect it. As $\mathrm{Cu_2O}$ content reaches 40 mol%, the conductivity jumps to 10^{-7} S $\mathrm{cm^{-1}}$ at 298 K. Similar observation has been made with the ternary glass as well. When the CuI content was less than 60 mol% and $\mathrm{Cu_2O}$ modifier content was less than 30 mol% of the total oxides, the conductivity was very low and could not be measured. The general tendency in conductivity variation of the ternary system is that the conductivity increases with addition of $\mathrm{Cu_2O}$ modifier when keeping the CuI content constant. We can see from log σ vs $1000/T$ plots that the slopes remain nearly independent of composition. Once the modifier concentration reaches a specific level, the glass begins to crystallize and then the slope changes considerably. This indicates that the conduction mechanism has changed with change in $\mathrm{Cu_2O}$ content. In the case of ternary system, the maximum conductivity is observed in the glass $0.70\mathrm{CuI}\cdot0.20\mathrm{Cu_2O}\cdot0.10\mathrm{TeO_2}$, in which CuI crystallites were found by XRD.

4. Discussion

4.1. XPS studies

XPS studies done on samples prepared by quenching the molten material in vacuum did not show

TABLE II The binding energy of core-level electrons in $xCu_2O\cdot(1-x)TeO_2$ glasses

x	O 1s(1)	O Is(2)	$F(A)$	Te 3d(1)	Te 3d(2)	Cu $2p_{3/2}$(1)	Cu $2p_{3/2}$(2)	Cu $2p_{1/2}$(1)	Cu $2p_{1/2}$(2)	F_{cu+}
0.1	527.2	529.6	0.056	573.0	575.2	932.0	933.5	951.0	953.8	0.242
0.2	528.1	530.4	0.055	574.0	576.0	932.0	934.3	951.7	954.3	0.131
0.3	528.3	530.5	0.086	573.6	575.9	932.0	934.1	951.0	954.0	0.061
0.4	530.2	531.4	0.349	573.0	575.8	933.1	934.4	952.1	954.5	0.234
0.5	530.3	531.3	0.718	572.8	575.8	932.6	934.4	951.9	954.3	0.364

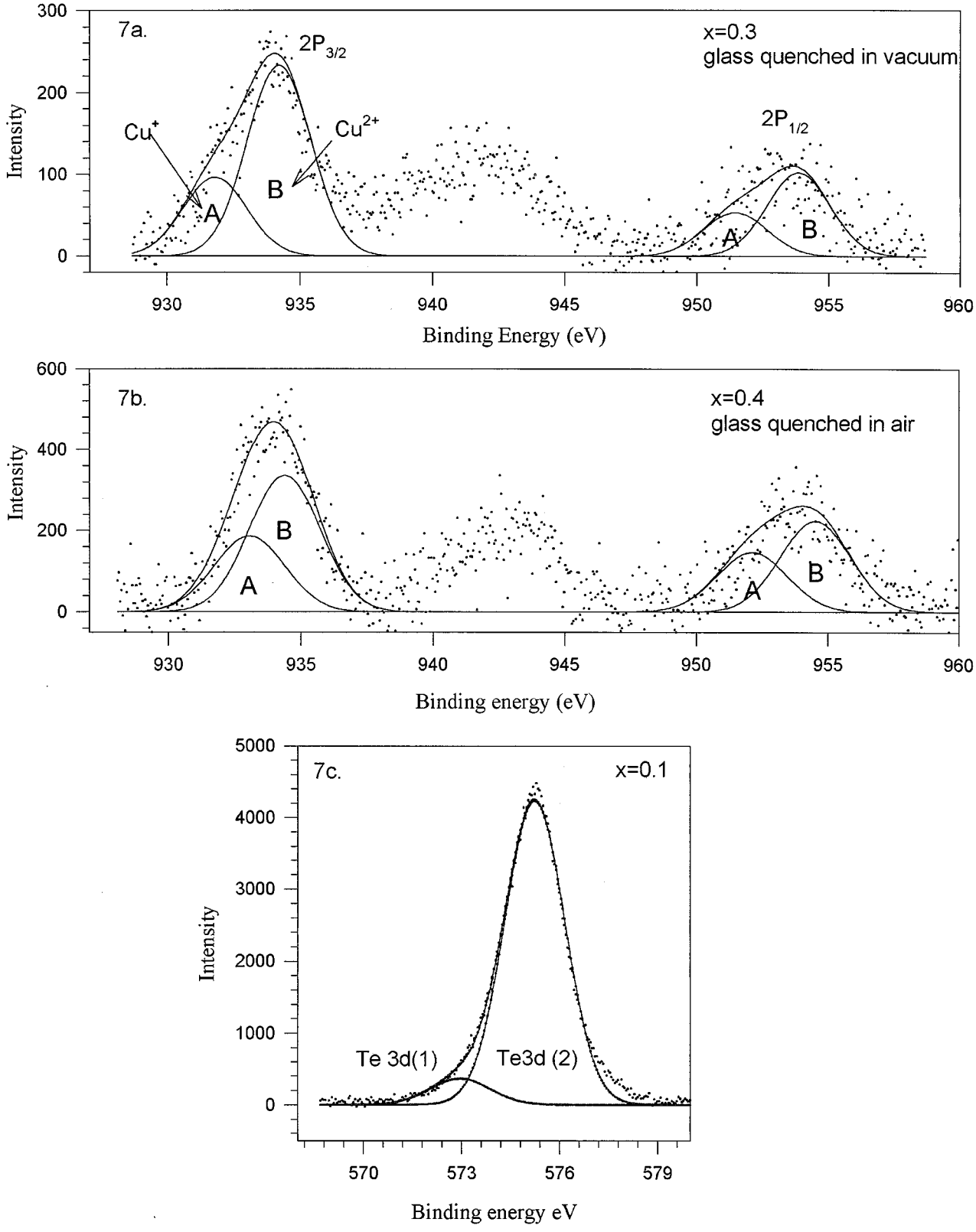

Figure 7 The XPS spectra of Te 3d and Cu 2p core electrons in the $xCu_2O\cdot(1-x)TeO_2$ glass system. (a) and (c) glasses quenching in air; (b) glass quenching in vacuum.

TABLE III The binding energy (eV) of core-level electrons in the xCuI.yCu_2O.$(1-x-y)TeO_2$ glasses

x	y	O 1s(1)	O 1s(2)	$F(A)$	Te3d(1)	Te 3d(2)	Cu $2p_{3/2}$(1)	Cu $2p_{3/2}$(2)	Cu $2p_{1/2}$(1)	Cu $2p_{1/2}$(2)	F_{cu+}	I 3d
0.4	0		530.4	0	573.2	575.9	932.2	934.5	951.8	954.2	0.433	619.2
0.4	0.1	528.5	530.6	0.067	572.8	575.8	932.3	934.5	951.8	954.1	0.528	619.2
0.4	0.2	528.6	530.8	0.059	572.5	575.8	932.1	934.7	951.9	954.5	0.648	619.2
0.4	0.3	530.7	531.8	0.923	574.0	575.8	932.1	934.7	951.9	954.5	0.603	619.2
0.5	0		530.4	0	572.5	575.7	932.2	934.3	952.0	954.2	0.333	619.1
0.5	0.1		530.5	0	572.6	576.0	932.1	934.3	951.9	954.5	0.743	619.3
0.5	0.2	530.6	531.5	0.624	572.3	575.8	932.4	934.6	952.2	954.7	0.508	619.6
0.5	0.3	530.7	532.1	0.910	572.5	575.5	932.4	934.7	952.3	954.9	0.657	619.6
0.6	0		530.7	0	572.6	575.8	932.7	934.8	952.4	954.7	0.399	619.2
0.6	0.1		531.5	0	573.0	575.8	932.5	934.6	952.2	954.4	0.436	619.4
0.6	0.2	530.1	531.8	0.659	572.5	576.0	932.4	934.7	952.2	955.0	0.696	619.6
0.7	0		530.8	0	572.6	575.8	932.2	934.4	952.1	954.5	0.508	619.3
0.7	0.1	529.8	530.4	0.687	571.2	575.0	931.4	933.8	951.2	953.7	0.616	619.5

significant difference in the relative concentration of Cu^+ and Cu^{2+} (Fig. 7a and b). Hence most of our studies are confined to samples that are melted in vacuum and quenched in air.

As mentioned earlier, each of the Cu $2p_{3/2}$ and Cu $2p_{1/2}$ peaks at 934 and 954 eV has been fitted into two peaks labeled as A and B (Fig. 7a and b). Based on earlier studies [22, 23], the peak A and B could be assigned to Cu^+ and Cu^{2+}, respectively. It is well known that the divalent Cu 2p peaks have two satellite peaks located at about 10 eV higher binding energy as compared to the main peaks at about 934 eV and 954 eV, and their intensity changes with change in intensity of main peaks [23]. Thus the peak at about 942 eV, shown in Fig. 7, is considered as the satellite peak of $2p_{3/2}$ (934 eV) peak which has been assigned to Cu^{2+}. It is clear that some of the copper ions changed their oxidation state from monovalent to divalent in the binary glass. The area ratios of peak A to the sum of areas of peaks A, B and the satellite, defined as F_{Cu+}, are also given in Table II and it is a measure of the Cu^+ quantity. It was found that maximum values of F_{cu^+} for Cu_2O-TeO_2 and CuI-Cu_2O-TeO_2 systems were 0.364 and 0.696 respectively.

Although it has been considered that amorphous TeO_2 consists of a three dimensional network of TeO_4 structural units [24], the O 1s spectra of α-TeO_2 crystal or TeO_2 glass show only one peak located at 530.2 eV. This implies that the electrons of the oxygen ions in the axial and the equatorial positions have the same binding energy. As Cu_2O is introduced into the TeO_4 glass network, the network is modified and some new bonds such as Cu^+-$_{eq}$O-Te, Cu^+-$_{ax}$O-Te and Te = O are created. However, we found that the O 1s peak could only be fitted into two peaks labeled earlier as O 1s(1) and O 1s(2) (Fig. 6). In non-bridging oxygen bonds (NBO), the charge distribution of electrons is displaced toward the oxygen atom causing the electron density surrounding the oxygen to increase, which results in lowering the nuclear potential and consequently a lower binding energy for the core electrons of the oxygen. Thus O 1s(1) and O 1s(2) peaks are assigned to the non-bridging and the bridging oxygen (BO) of the structural units, respectively. It was found that in the binary system the peak area ratio of O 1s(1) to total O 1s, referred earlier as $F(A)$, is only about 0.055 when x is less than 0.3 (Table II). This value is too low as compared to that observed for other binary systems suggesting that the number of NBOs in the $Cu_2O{\cdot}TeO_2$ glass system is relatively low.

Based on earlier studies on alkaline earth oxide based system [25], NBOs should also increase with the increase in concentration of divalent copper. Since it has been already confirmed that Cu^{2+} is present in high content in the presently investigated glass samples, in addition to Cu^+ ions forming the bonds of Te-$O^-_{eq}Cu^+$ and Te-$O^-_{ax}Cu^+$, we assume that the divalent copper ions will also modify the structural units to form bonds like Te-$O^-_{eq}Cu^{2+}$ and Te-$O^-_{ax}Cu^{2+}$. In order to maintain electrical neutrality, Cu^{2+} ions must bond with second oxygen from other structural units to form O^--Cu^{2+}-O^- linkage. Thus we believe that the oxygen bonding to Cu^{2+} would have similar electron density as BO, and hence the core electrons from Cu^{2+}-related oxygen will contribute to O 1s(2) peak instead of O 1s(1) peak, while O 1s(1) is only associated with core electrons of oxygen terminated with Cu^+ and double bonded oxygen (Te=O). Accordingly, we find that only when x is greater than 0.4 or $F_{Cu+} > 0.3$, the fractional concentration of NBO (i.e., O 1s(1) peak, intensity) increases to 0.349 (Fig. 6 and Table II).

The intensity and binding energy of NBO and BO in the ternary glasses show almost the same behavior as those in the binary system. This fact indicates that the oxygen atoms in the ternary system have similar local atomic coordination as in the binary glass, and we can expect that the iodine ions are not participating in the network formed by copper and tellurium oxides. Otherwise, due to large difference between the oxygen electronegativity (3.5) and iodine electronegativity (2.2), the binding energy of O 1s should shift. The only difference presently observed between the binary and ternary systems is that the average Cu^+ fraction is higher in ternary system than that in the binary system. It is likely that the ternary system has relatively high ability to prevent oxidation of the monovalent copper ions. But since all glasses prepared in the ternary system have more than 40 mol% CuI, high Cu^+ concentration may also be helpful to stabilize monovalent copper ions.

Among the Te 3d(1) and Te 3d(2) peaks at 573 and 575 eV, respectively, the Te 3d(2) is unambiguously associated with main structural units like TeO_3^{2-}, TeO_3^-

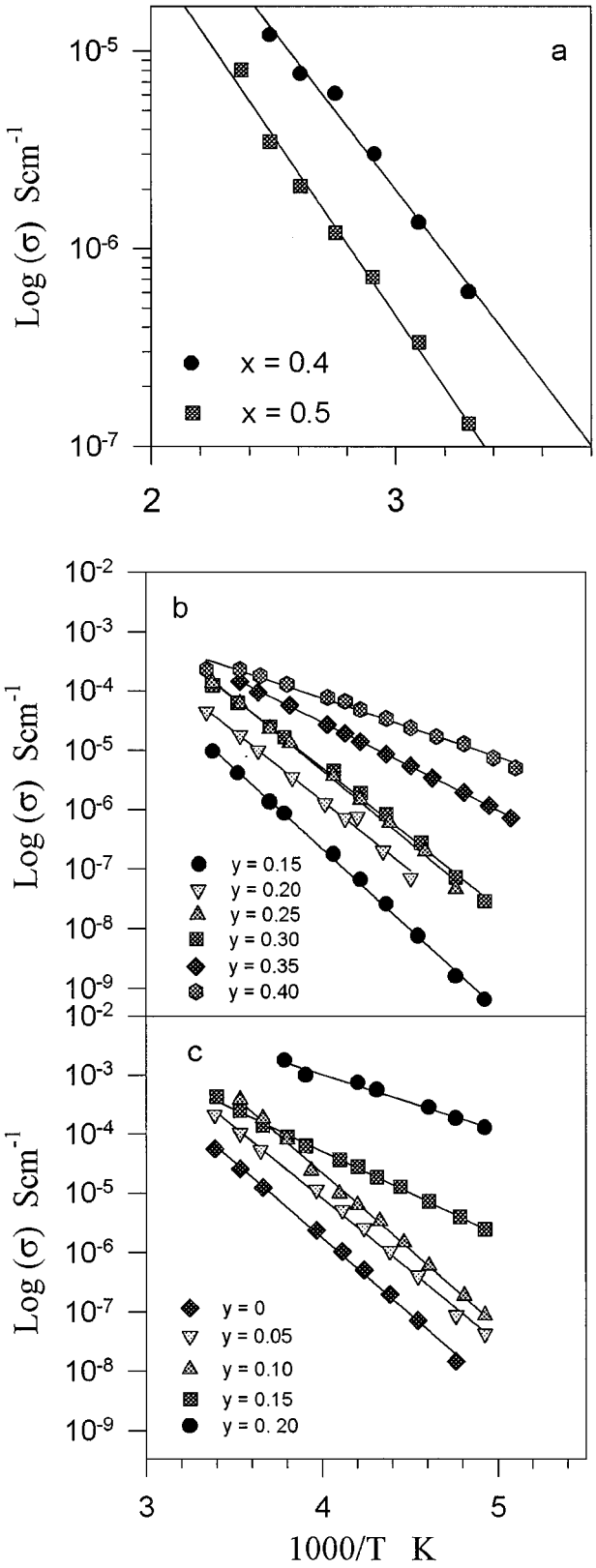

Figure 8 The temperature dependence of the conductivity of (a) xCu$_2$O·(1 − x)TeO$_2$; (b) 0.4CuI·yCu$_2$O·(0.6 − y)TeO$_2$; and (c) 0.7CuI·yCu$_2$O·(0.3 − y)TeO$_2$.

and TeO_4, etc. The Te 3d(1) peak is only a small fraction of the total Te 3d peak and the average ratio of area of Te 3d(1) to Te 3d peak is less than 0.12. Referring to a similar situation we encountered earlier [26], we attribute this peak to the formation of Cu-Te bond since Cu^+ has ionic radius = 0.96 A and electronegativity = 1.8 and the ion may lie close to the NBO site, thus causing overlapping of electron wavefunctions of copper and tellurium. Further, the electrons from copper 3d-obital will also participate in bonding and hence cause an increase in the covalence of Cu-X (X = O, I, Cl, Te, etc.) bonds. However, we find that this Te 3d(1) bond does not show a clear relationship to the added modifier concentration.

The nature of the Cu-Te bond in the ternary system is found to be the same as that in the binary system. The average fraction of Te 3d(1) is about 0.1. The binding energy of I 3d electrons shows very little change within the range of 0.6 eV. This also reflects the stable coordination of iodine ions in glasses.

4.2. Raman study

As has been discussed earlier, the Raman spectra of the $Cu_2O{\cdot}TeO_2$ can be fitted mainly five Gaussian bands, represented as A, B, C, D and E as shown in Fig. 5 [7, 12, 20]. The band A located at about 780 cm^{-1} and the band B observed at about 720 cm^{-1} are assigned to the stretching mode of TeO_3 (tp) with NBOs and the vibration of the continuous TeO_4 (tbp) network respectively. The bands C and D observed at about 660 and 620 cm^{-1}, respectively, are ascribed to the stretching mode of TeO_4 (tbp) with BO. Located at 440 cm^{-1} is the band E, which is attributed to a symmetric bending vibration of Te-O-Te vertex linkages between different TeO_4 (tbp), TeO_{3+1} polyhedra. Thus the band E is an indication of continuity of tellurite structural units in glass.

The intensity change of different vibration bands reflects the change in structural units in a glass [7]. When a modifier is introduced, the structural units of tellurite glass will have some changes in the TeO_4 units producing TeO_3 (tp) with doubly bonded oxygen represented by the equation:

$$TeO_4 \Leftrightarrow O_{2/2}Te{=}O \tag{1}$$

Other possibilities include formation of TeO_3^- of the configuration $O_{3/2}TeO^-$ in which NBO is terminated by modifier cation. The latter configuration may be further modified as:

$$O_{3/2}TeO^- \Rightarrow O_{1/2}Te(=O)O^- \tag{2}$$

Following this vitrification mechanism, the model can be formulated as:

$$\begin{aligned} xO^{2-} + TeO_{4/2} \Leftrightarrow 2x\{&a[O_{3/2}Te - O^-] \\ &+ b[O_{1/2}Te(=O) - O^-]\} \\ &+ cx[O_{2/2}Te{=}O] + (1 - 2x - cx)TeO_{4/2} \end{aligned} \tag{3}$$

The values a, b and c are less than 1 and sum of a and b equals to 1. From this model, the ratio of TeO_3 and TeO_4 could be estimated as a function of the atomic O/Te ratio:

$$\frac{TeO_3}{TeO_4} = \frac{(2b + c)([O/Te] - 2)}{\{1 - (2b + c)([O/Te] - 2)\}} \tag{4}$$

The ratio of NBO and BO could also be calculated as:

$$\frac{\text{NBO}}{\text{BO}+\text{NBO}} = \frac{(2[\text{O/Te}]-3)[\text{TeO}_3/\text{TeO}_4]+2[\text{O/Te}]-4}{[\text{O/Te}]([\text{TeO}_3/\text{TeO}_4]+1)} \quad (5)$$

The ratio of the concentration of TeO_3 and TeO_4 units can be estimated from the intensity ratio of 780 and 660 cm^{-1} bands in the Raman spectra. But as we know pure TeO_2 glass that contains only TeO_4 units exhibits 780 cm^{-1} bands suggesting that these units also contribute to the intesnity of 780 cm^{-1} bands. Thus while 660 cm^{-1} bands in modified system is exclusively due to TeO_4 units, the 780 cm^{-1} band is due to both TeO_4 and TeO_3 units. Thus any increase in the intensity ratio of 780 and 660 cm^{-1} bands should invariably be associated with increase in TeO_3 units and decrease in TeO_4 units. Therefore, in order to estimate the minimum number of TeO_3 units that are present in the modified system, we have subtracted the intensity ratio of 780 and 660 cm^{-1} bands of the pure system from that of modified system. Since it is impossible to prepare pure TeO_2 glass, in order to estimate the intensity ratio of 780 and 660 cm^{-1} bands in pure glass system, we have extrapolated the plot of I_{780}/I_{660} vs. O/Te of modified system to O/Te = 2 and taken that value as a measure of the concentration of TeO_4 units in pure system A plot of I_{780}/I_{660} after having subtracted the data of pure system as a function of oxygen and tellurium ratio is shown in Fig. 9. The intensity ratio of TeO_3 and TeO_4 units has also been calculated using the formula discussed earlier (Equation 4) choosing different *a*, *b* and *c* values and the data as a function of O/Te is also shown in Fig. 9a and b.

From this figure it is reasonable to conclude that as *x* is within 0.1 to 0.3, the *c* value is ≤ 0.6 i.e., the network contains a fraction of $O_{2/2}Te=O$ units, since with low *x* value *b* should be relatively small and thus dominant structural units should be $O_{3/2}TeO^-$ and $O_{2/2}Te=O$. As *x* increases to 0.4 or more, *c* becomes close to zero and hence almost no $O_{2/2}Te=O$ units remain. Instead, the network is mainly composed of $O_{3/2}TeO^-$ and $O_{1/2}Te(=O)\text{-}O^-$ units. The structural unit ratio of *a* and *b* is in the range of 1.5 to 9 as can be seen from Fig. 9. It is clear that these parameters do not represent the real vitrification mechanism because many combinations of *a*, *b* and *c* parameters also can fit to these experimental data. However, these parameters can give an estimation of relative ratio of different structural units in the network.

The ratio of NBO to total oxygen content was calculated by making use of the intensity ratio of TeO_3 and TeO_4 for a given O/Te ratio (Equation 5). NBO/(NBO + BO) ratio calculated from both Raman data and XPS spectra are plotted in Fig. 10a. It is obvious that the ratio of NBO to total oxygen content obtained from Raman data is higher than that obtained from XPS data. The reason for this is that NBO fraction calculated from intensity ratio (extracted) of 780 and 660 cm^{-1} bands contains *all* non bridging oxygen atoms whether they are double bonded or, Cu^+ or Cu^{2+} terminated. On the contrary, as explained in previous section, the NBO fractions calculated from XPS spectra are those of oxygen atoms double bonded and terminated by monovalent copper ions. This means that divalent copper atoms, which form $O\text{-}Cu^{2+}\text{-}O$ bonds, cause the difference between those two curves.

As Cu_2O content increases to more than 40 mol%, a new band is observed at 400 cm^{-1} (F in Fig. 5). Based on the published Raman data in alkali tellurite glass [27], this band is assigned to TeO_3 with two or more NBO. The appearance of this band strongly supports the above assignment. Comparing to the similar band in alkali tellurite glass (330 cm^{-1}), this band shifts to high fequency side and this can be explained by different valence electrons and higher electronegativity of copper ions, hence having different coordination to NBO atoms.

It was noted that as *x* is greater than 0.3, the Raman band D at 620 cm^{-1} tends to increase in intensity. Quantitatively the intensity ratio of 620 and 660 cm^{-1} bands (D and C) changes from 0.789 to 4.155 as *x* increases from 0.3 to 0.5. This result is quite different from that observed in alkaline tellurite glass system. To account for this difference, we cite the mechanism proposed by Sekiya *et al.* [28] for MgO-TeO_2 system. As MgO conent increases to more than 40 mol%, a $(Te_3O_8^{4-})_n$ unit is formed in glass network. The $(Te_3O_8^{4-})_n$ unit is composed of TeO_4 with two TeO_3 ends as shown in Fig. 11. Thus we assume that as cuprous oxide content increases to more than 0.3 the glass begins to form $(Te_3O_8^{4-})_n$ units. The intensity of the band C (660 cm^{-1}) decreases as *x* increases and this is the result of formation of $(Te_3O_8^{4-})_n$ units, which means the number of TeO_3 species increases. At the same time this indicates that *n* is relatively small. When *x* continues to increase, the $(Te_3O_8^{4-})_n$ units tend to bind to adjacent nearby tellurium atom through TeO_3 to form $(Te_3O_8^{4-})_n$ chain. At the same time as mentioned previously, Cu^{2+} ions probably form $^-O\text{-}Cu^{2+}\text{-}O^-$ bonds, which cause equivalent TeO_4 unit network. This is the main reason for causing the band D to increase in intensity so fast, since TeO_4 network connected through -O-Cu^{2+}-O- has different polarization from that of the free network TeO_4.

By the same method, the TeO_3/TeO_4 ratio of the ternary system is estimated from Raman experiments and calculated from Equation 4 given earlier, as shown in Fig. 9c and d. It is found that although the glasses are with different CuI content, the TeO_3/TeO_4 ratio has very similar values. Thus we may conclude that the oxide structural units are seldom affected by the presence of iodine ions. But by comparing to binary system, it is clear that the *c* value has relatively increased. This means that in the ternary system more number of TeO_3 units contain double bonded oxygen. Since the phase separation occurs in the ternary glass and the glass has vast interface between CuI glass and oxide glass, we assume that the structural units on surface of oxide glass droplets can bond with Cu^+ or Cu^{2+} ions of halide glass. Then it is reasonable to suppose that inside the oxide network the structure still keeps relatively more

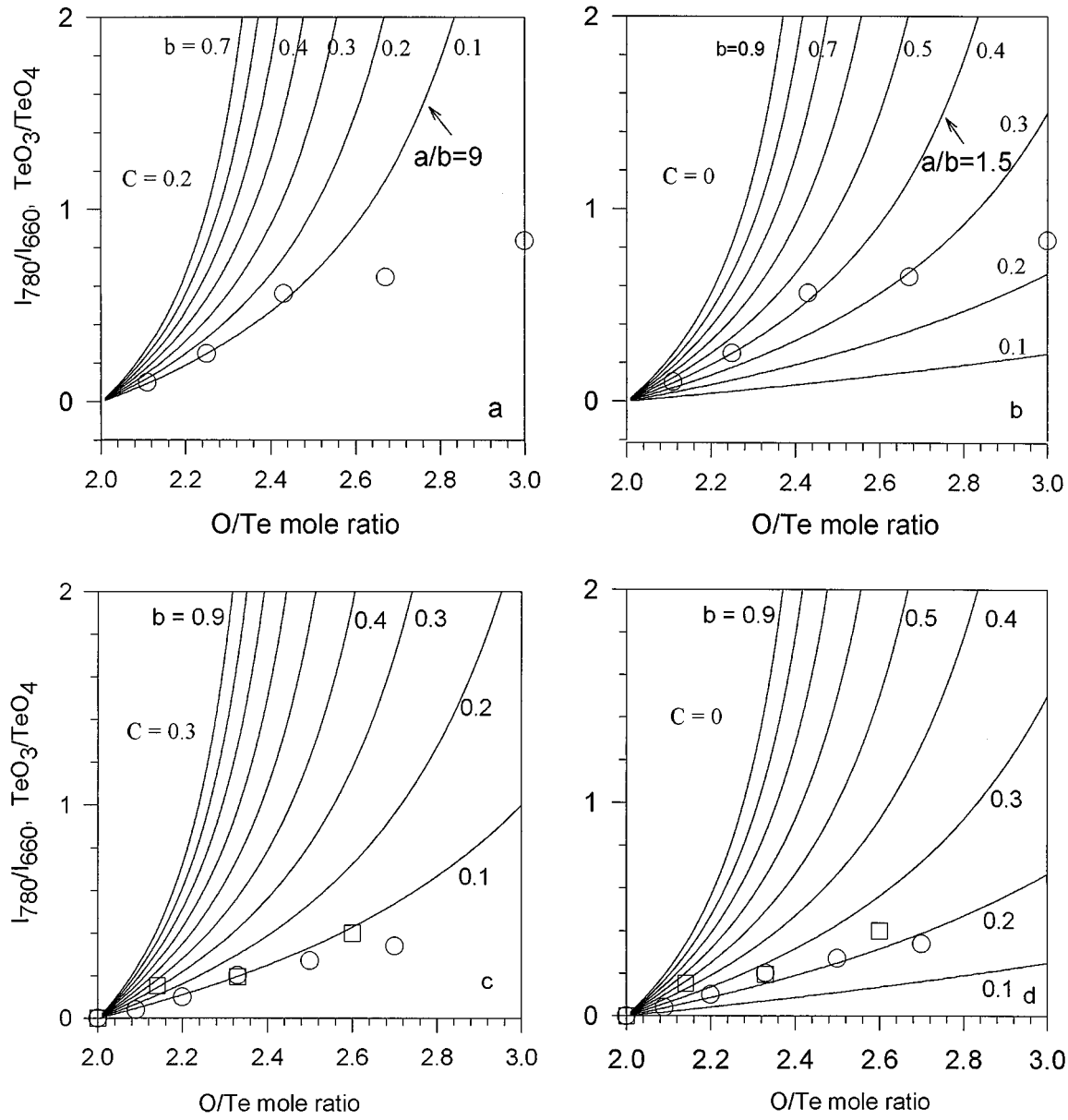

Figure 9 The TeO_3/TeO_4 ratio estimated from the Equation (4) as a function of O/Te and the Raman experimental data I_{780}/I_{660}. (a) $c = 0.2$ and (b) $c = 0$ of $x Cu_2O \cdot (1-x) TeO_2$ glasses experimental data points fit with the calculated curves for a/b ratio 1.5 ~ 9. (c) $c = 0.3$ and (d) $c = 0$ of $x CuI \cdot y Cu_2O \cdot (1-x-y) TeO_2$ [$x = 0.4$ (○) and 0.6 (□)].

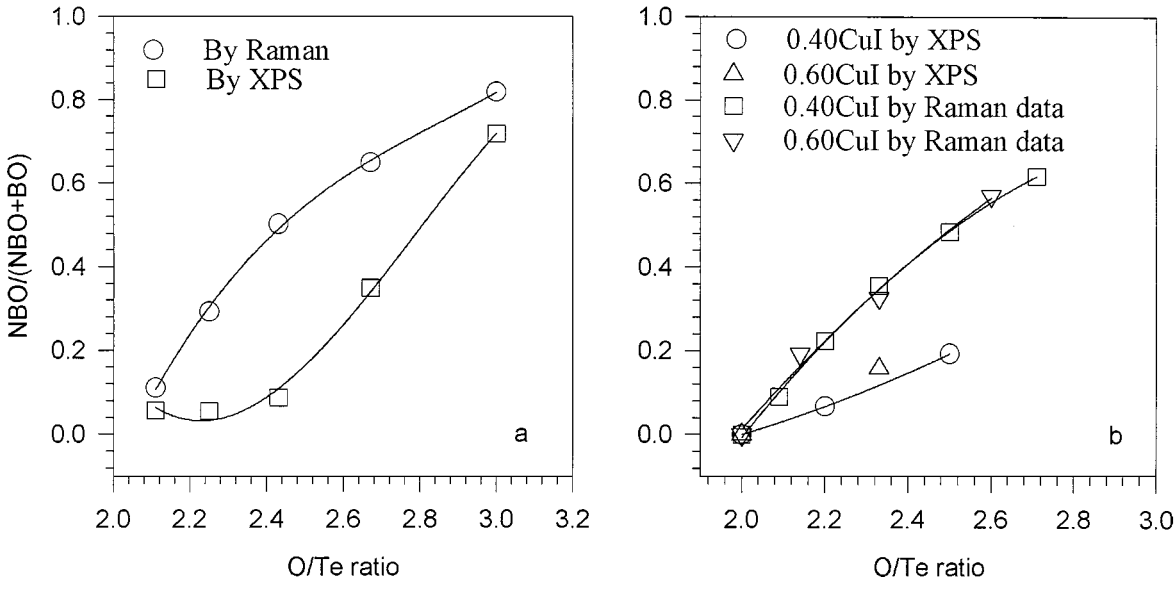

Figure 10 The comparison of NBO fraction obtained from Raman and XPS measurements. (a) $x Cu_2O \cdot (1-x) TeO_2$ (b) $x CuI \cdot y Cu_2O \cdot (1-x-y) TeO_2$.

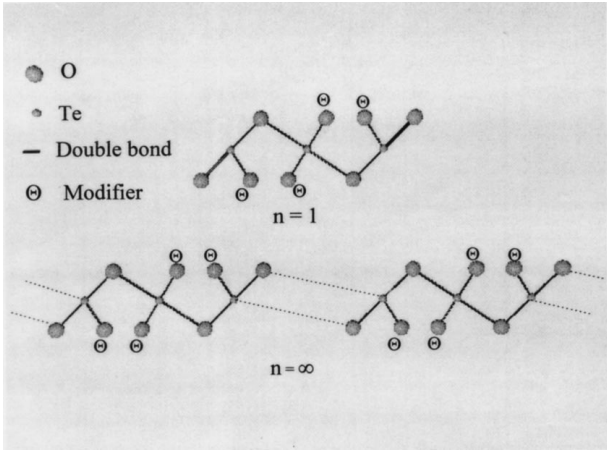

Figure 11 The schematic figure of ($Te_3O_8^{4-}$) structural unit.

bridging oxygen. This may also be the reason why we didn't find the intensity of Raman band D(620 cm^{-1}) increasing with increase in Cu_2O content as observed in the glasses of the binary system with high Cu_2O content. Therefore, it is not necessary to form $(Te_3O_8^{4-})_n$ structural units to satisfy the bonding requirement and instead the interface bonding can compensate this part.

The fraction of NBO of the ternary system, estimated by the above method, is shown in Fig. 10b. The fraction calculated from Raman experiments shows very good consistency. The basic structural units in network are only concerned with the oxygen to tellurium ratio and it has almost no effect by addition of the cuprous iodide. The NBO fractions obtained from XPS data, like the binary system, show a relatively low value. It is reasonable to explain this result by the same assumption as in the binary system.

4.3. Electrical conductivity and phase separation

The conductivity of the $xCu_2O{\cdot}(1-x)TeO_2$ glass system is controlled by the concentration of monovalent copper ions in glass and the glass structure. When x is within 0.1 and 0.3, no ionic conduction can be found and their electronic conduction is also in the range of 10^{-11} to 10^{-14} S cm^{-1}. From the XPS results we have found that the Cu^+ concentration (per mole) is less than 0.06 and NBO fraction in glasses with $x \leq 0.3$ is only around 0.055. The binding energy of NBO is about 2 eV lower than that in glasses with $x \geq 0.4$. This is directly correlated with the high electron density around NBO and hence the NBOs strictly trap the monovalent copper ions. This may cause increase of the electrostatic binding energy E_σ, which prevents the hopping of a mobile ion from the vicinity of NBO position [29, 30]. As x increases to more than 0.4, Cu^+ number increases to more than 0.29 (per mole) and at the same time NBO fraction increases from about 0.055 to above 0.349. It is believed that it is the result of formation of $(Te_3O_8^{4-})_n$ structural unit in glass. Also, the binding energy of O 1s(1) shifts to high energy, which may lead to lower electrostatic binding energy of Cu^+ to NBOs. Thus it seems that $x = 0.3$ is a critical point, above which the ionic conductivity increases significantly while at the same time the electronic conductivity also increases to the level of 10^{-9} S cm^{-1}.

Ternary system $CuI{\cdot}Cu_2O{\cdot}TeO_2$ had relatively higher ionic conductivity as compared with the $Cu_2O{\cdot}TeO_2$ binary system since the ternary system had cuprous iodide which itself has high ionic conductivity. In this system too we have found the same situation as in the binary system: when CuI content was less than 60%, no ionic conduction could be measured if Cu_2O modifier content is less than 30 mol% (here the mole percentage is calculated as $\frac{Cu_2O}{Cu_2O+TeO_2}$).

From AFM study, also we found that the phase separation occurs in the ternary system with high CuI content. The main structural character of these glasses may be visualized by considering that these glasses are made up of numerous droplets and these droplets form different size clusters depending on the composition as shown in Fig. 4. These droplets are believed to be oxide glass phase. It is measured that in the glass of $0.4CuI{\cdot}0.6TeO_2$ the average droplet size is about 60.5 nm and the average cluster size is about 820.4 nm (Fig. 4a and b). The glass of $0.4\,CuI{\cdot}0.2Cu_2O{\cdot}0.4TeO_2$ has its average droplet size 35.4 nm and the average cluster size about 120.3 nm (Fig. 4c). Thus we can see that the microstructure is controlled by the chemical composition.

According to the proposed phase separation model [13], glass containing a copper halide is easy to get phase separated with one of the phases being halide. With different volume ratio and different morphology of the two phases, the conductivity can change by a large magnitude. Since the percolation theory [31] indicates that there exists a critical threshold P_c, below which the small-volume phase is isolated and above it the isolated phase becomes connected. However, this critical point is not a universal parameter and it is controlled by many factors of the system. In the present case a modifier content (Cu_2O) is less than 30 mol% and CuI content is less than 50 mol%, the halide phase is in an isolated state. Thus the conduction should be carried out by large volume phase of $Cu_2O{\cdot}TeO_2$ glass alone. As seen in the binary system, no ionic conduction has been observed in binary system with $Cu_2O \leq 30$ mol% and hence the ternary system with $\frac{Cu_2O}{Cu_2O+TeO_2} \leq 30$ mol% and CuI ≤ 50 mol% does not show ionic conduction. When Cu_2O modifier content is >30 mol%, the morphology of halide phase changes from isolated sate to continuous pathway. Apparently the ionic conductivity jumps drastically to 10^{-4} S cm^{-1} at 298 K. When CuI content is high enough (in this case above 60 mol%), the halide volume percentage is higher than the oxide glass and it may already form a continuous network. Then even when no Cu_2O modifier is added to the glasses, ionic conductivity has high value. Thus, the electrical conductivity data provided indirect experimental evidence to support the phase separation model. Earlier, Tatsumisago *et al.* [32] also found that the AgI-rich amorphous particles with 40–60 nm in diameter were dispersed in the twin-roller quenched and iron-press quenched glass systems $AgI{\cdot}Ag_2O{\cdot}M_xO_y$($M_xO_y = B_2O_3$, GeO_2,

WO_3) with 70–75 mol AgI. Thus we believe that the phase separation might be a common phenomenon in halide doped oxide glass systems prepared by quenching at high rate. But to understand this further, many experiments have to be done especially with respect to glass microstructure.

It is found that with high content of Cu_2O and CuI, the α-CuI phase can be stabilized at room temperature. In the composition region studied, we did not find β-CuI crystalline phase in the glass. The glass specimens with α-CuI crystallites show very high conductivity (up to 4.21×10^{-3} S cm^{-1} at 298 K; Fig. 8 and Table I). The stabilization of α-CuI in the present system is similar to the stabilization of α-AgI in $AgI{\cdot}Ag_2O{\cdot}B_2O_3$ system reported by Tatsumisago *et al.* [33, 34]. It is believed that the reason for this kind of crystallite stabilization is that the glass matrix has a strong suppression effect of the phase transformation, which keeps α-CuI phase to room temperature in the fast quenching process. The estimated average diameter of α-CuI crystallites is about 104.8 nm. It may be stated that this is a common phenomenon in ZrO_2 toughened ceramic composites; the tetragonal ZrO_2 phase has been stabilized only when the particle size is below the critical size of $0.1 \sim 1\,\mu$m [35].

5. Conclusions

XPS, Raman spectroscopy, AFM, and electrical conductivity analysis studies have been done on the $x Cu_2O{\cdot}(1-x)TeO_2$ and $x CuI(1-x)[y Cu_2O(1-y)TeO_2]$ glass systems. Based on the studies the following conclusions have been drawn. In the $x Cu_2O{\cdot}(1-x)TeO_2$ system, monovalent cuprous ions have very high tendency to oxidize (to Cu^{2+}) when x is lower than 0.3. Only when x is above 0.4, the glasses show ionic conduction due to Cu^+ ions. In the network of the binary system, Cu^{2+} ions form O-Cu^{2+}-O bond and this contributes to the XPS peak ascribed to bridging oxygen. It is also found that the $(Te_3O_8^{4-})_n$ structural unit is formed in glass when $x \geq 0.4$. From all aspects of study, we conclude that the CuI-Cu_2O-TeO_2 is a phase-separated system. Its structure is controlled by the chemical composition and hence the glasses show different conduction behavior. In the ternary system, α-CuI has been stabilized at room temperature by the glass matrix and this leads to high ionic conductivity.

Acknowledgement

The authors wish to thank Dr. Shen Zhixian for his support in Raman study and Mr. H. K. Wong for his help in taking the XPS spectra. The authors have benefited immensely from the discussion with Prof. G. V. Subba Rao, Institute of Materials Research and Engineering (IMRE), Singapore.

References

1. J. L. SOUQUET and M. DUCLOT, in "Trends in Materials Science," MiMS-97, edited by S. Radhakrishna (Narosa Publishing House, 1997) p. 232.
2. T. MINAMI, *Bull.Inst. Chem. Res.*, Kyoto.Univ. **72** (1994) 127.
3. "CRC Handbook of Chemistry and Physics," 67th ed., Section F, 1987.
4. T. MINAMI and N. MACHIDA, *Materials Chemistry and Physics* **23** (1989) 63.
5. N. MACHIDA, M. CHUSHO and T. MINAMI, *J. Non-Cryst. Sol.* **101** (1988) 70.
6. T. SEKIYA, N. MOCHIDA, A. OHTSUKA and M. TONOKAWA, *ibid.* **144** (1992) 128.
7. Y. HIMEI, A. OSAKA, T. NANBA and Y. MIURA, *ibid.* **177** (1994) 164.
8. K. TANAKA, T. YOKO, H. YAMADA and K. KAMIYA, *ibid.* **103** (1988) 250.
9. M. D. PANKOVA, Y. DIMITRIEV, M. ARNAUDOV and V. DIMITROV, *Phys. and Chem. of Glasses* **30** (1989) 260.
10. J. M. ROJO, J. SANZ, J. M. REAU and B. TANGUY, *J. Non-Cryst. Sol.* **116** (1990) 167.
11. M. TATSUMISAGO, S. K. LEE, T. MINAMI and Y. KOWADA, *ibid.* **177** (1994) 154.
12. M. TATSUMISAGO, T. MINAMI, Y. KOWADA and H. ADACHI, *Phys. & Chem. Glasses* **35** (1994) 89.
13. B. V. R. CHOWDARI, K. L. TAN and L. FANG, *Solid State Ionics*, to be published.
14. X. B. WANG, Z. X. SHEN, C. K. ONG, S. H. TANG and M. H. KUOK, in XV International Conf. on Raman Spectroscopy, Univ. Pittsburgh, August 1996, p. 762.
15. S. CHANDRA, "Superionic Solids, Principles and Applications" (North-Holland, 1981) p. 143.
16. S. N. MAGONOV, "Surface Analysis with ATM and AFM" (VCH, 1996).
17. T. YOKO, K. KAMIYA, H. YAMADA and K. TANAKA, *J. Amer. Ceram. Soc.* **71** (1988) C70.
18. S. ROSSIGNOL, J. M. REAU, B. TANGUY, J. J. VIDEAU and J. PORTIER, *J. Non-Cryst. Sol.* **155** (1993) 77.
19. Q. J. RONG, A. OSAKA, T. NANBA and J. TAKEDA, *J. Mater. Sci.* **27** (1992) 3793.
20. T. SEKIYA, N. MOCHIDA, A. OHTSUKA and M. TONOKAWA, *J. Non-Cryst. Sol.* **144** (1992) 128.
21. Y. HIMEI, Y. MIURA, T. NANBA and A. OSAKA, *ibid.* **211** (1997) 64.
22. M. A. SALIM, G. D. KHATTAK and M. S. HUSSAIN, *ibid.* **185** (1995) 101.
23. D. BRIGGS and M. P. SEAH, "Practical Surface Analysis" (John Wiley & Sons, 1994) p. 362.
24. T. SEKIYA, N. MOCHIDA, A. OHTSUKA and M. TONOKAWA, *J. Ceram. Soc. Jpn.* **97** (1989) 1435.
25. R. K. BROW, *J. Non-Cryst. Sol.* **194** (1996) 267.
26. B. V. R. CHOWDARI and P. P. KUMARI, *ibid.* **197** (1996) 31.
27. T. SEKIYA, N. MOCHIDA and A. SOEJIMA, *ibid.* **191** (1995) 115.
28. T. SEKIYA, N. MOCHIDA and A. OHTSUKA, *ibid.* **168** (1994) 106.
29. O. L. ANDERSON and D. A. STUART, *J. Amer. Ceram. Soc.* **37** (1954) 573.
30. S. W. MARTIN, *ibid.* **74** (1991) 1767.
31. J. FEDER, *Fractals*, Plenum Press, 1988, p. 104.
32. M. TASUMISAGO, K. OKUDA, N. ITAKURA and T. MINAMI, in Extented Abstracts of 11th Inter.Conf. on Solid State Ionics, Honolulu, Hawaii, USA, November 16–21, 1997.
33. M. TATSUMISAGO, Y. SHINKUMA and T. MINAMI, *Nature* (London) **354** (1991) 217.
34. T. SAITO, M. TASUMISAGO, N. TORATA and T. MINAMI, *Solid State Ionics* **79** (1995) 279.
35. E. A. G. HEUER, *J. Amer. Ceram. Soc.* **63** (1980) 241.

Received 30 July 1998
and accepted 15 June 1999